Nanoscale

PAPER

View Article Online
View Journal | View Issue

Cite this: *Nanoscale*, 2014, **6**, 8177

Extraction of light trapped due to total internal reflection using porous high refractive index nanoparticle films

Peng Mao,[a] Fangfang Sun,[bc] Hanchao Yao,[a] Jing Chen,[a] Bo Zhao,[a] Bo Xie,[a] Min Han*[a] and Guanghou Wang[a]

Received 26th February 2014
Accepted 9th April 2014

DOI: 10.1039/c4nr01065e

www.rsc.org/nanoscale

TiO_2 nanoparticle layers composed of columnar TiO_2 nanoparticle piles separated with nanoscale pores were fabricated on the bottom surface of the hemispherical glass prism by performing gas phase cluster beam deposition at glancing incidence. The porosity as well as the refractive index of the nanoparticle layer was precisely tuned by the incident angle. Effective extraction of the light trapped in the substrate due to total internal reflection with the TiO_2 nanoparticle layers was demonstrated and the extraction efficiency was found to increase with the porosity. An enhanced Rayleigh scattering mechanism, which results from the columnar aggregation of the nanoparticles as well as the strong contrast in the refractive index between pores and TiO_2 nanoparticles in the nanoporous structures, was proposed. The porous TiO_2 nanoparticle coatings were fabricated on the surface of GaN LEDs to enhance their light output. A nearly 92% PL enhancement as well as a 30% EL enhancement was observed. For LED applications, the enhanced light extraction with the TiO_2 nanoparticle porous layers can be a supplement to the microscale texturing process for light extraction enhancement.

Introduction

Extensive studies have shown that efficiencies of optoelectronic devices largely depend on their structure design. Recently, various nano/microstructures for efficient and effective photon management have been applied to photodetectors,[1] solar cells[2] and light emitting diodes.[3,4] These nano- to micro-scale surface modifications show impressive performance in optical response through merging the advantages of different feature sizes.

Total internal reflection (TIR) at the semiconductor–air interface results in poor light extraction efficiency from light emitting devices. Due to the high-refractive-index contrast, the angle of the light escape cone for the semiconductor–air interface is very small. For example, the critical angle θ_c, given by Snell's law, for unencapsulated GaN ($n_{GaN} = 2.5$), is only about 23°. Most of the light from the quantum wells is totally internally reflected at the LED and air interface, trapped inside the device and ultimately converted to heat,[5] resulting in a significant reduction in the light extraction efficiency. Only about 4% of the generated light can escape from the surface into free space.[6,7] An increase in the light extraction efficiency is considered to be crucial to improve the efficiencies of light emitting devices.

Several methods have been proposed to realize the optimal photon management for enhancing the light extraction efficiency of light emitting devices, which include photonic crystals,[8] conductive omnidirectional reflectors,[9] and surface roughening of indium tin oxide.[10] Most studies have focused on patterns of micrometer size due to the ease of fabrication, among which surface texturing and patterning of transparent electrodes are some of the commonly used effective methods. For example, the output power of GaN-based LEDs could be enhanced by 28% to 45% by texturing of the transparent p-type electrode.[3,4] However, the electrode texturing involves a dry-etching process, which could cause the degradation of the electrical properties of GaN-based LEDs. For next generation applications of high efficiency LEDs, further improvement of the light extraction efficiency is required.

Recently, nanoscale structures have been studied for improving the output power of LEDs. A six-layer graded-refractive index antireflection coating made of indium tin oxide (ITO) was fabricated on GaInN LEDs to replace the common dense ITO coating.[11] A light-extraction efficiency enhancement of 24.3% was achieved due to a strongly reduced Fresnel reflection at the ITO/air interface. Vertically aligned ZnO nanorod arrays were grown on the transparent electrode of GaN LEDs, the light output power of the LEDs exhibited an enhancement by up to 50%, in comparison with conventional LEDs.[12] With

[a]*Key Laboratory of Modern Acoustics and Department of Materials Science and Engineering, Nanjing University, Nanjing 210093, China. E-mail: sjhanmin@nju.edu.cn; Fax: +86-25-83686248; Tel: +86-25-83686248*

[b]*Immunology and Reproduction Biology Laboratory, Medical School, Nanjing University, Nanjing, 210093, China*

[c]*Institute and Hospital of Stomatology, Nanjing University Medical School, Nanjing, 210008, China*

syringe-like ZnO nanorods, a superior light extraction efficiency and a more collimated radiation pattern with a view angle collimated from 136° to 121° were realized by Hsiao *et al.*[13] LEDs grown on the nanoscale patterned sapphire substrates also exhibited higher external quantum efficiency enhancement relative to those grown on the microscale patterned sapphire substrates.[14] Typically, however, the preparation of nanoscale features requires complex and expensive processes, such as e-beam lithography, or may result in surface damage. For example, the forward voltage of GaN LEDs with ZnO nanorods was increased significantly due to thermal damage of the transparent p-electrode during ZnO nanorod growth at high temperature.[10,15] Furthermore, research studies have demonstrated that the nanostructures might provide an alternative or supplement to the microscale texturing process for light extraction enhancement. Recently, Ho *et al.*[16] showed that the hierarchical structure consisting of p-GaN microdomes and SiO_2 nanorods could generate much greater enhancement of the light output intensity of GaN LEDs, as compared with LEDs with only microscale roughness of p-GaN microdomes. However, until now the enhanced light-extraction effect of nanostructures is mainly attributed to the waveguiding effect, multiple tilted surfaces and the graded refractive indices provided by the structures.[13,16] As for the reduction of the TIR at the semiconductor–air interface, the application of nanostructures has scarcely been discussed. More detailed studies are necessary to clarify the fundamental problem of light extraction enhancement with nanostructures.

In this paper, we study the extraction of the light which is otherwise trapped by TIR in semiconductors with nanoparticles of high refractive index dielectric materials, typically TiO_2. TiO_2 microsphere arrays have been used to enable the optimization of the light extraction efficiency of the nitride LEDs by providing higher indices that can result in larger light coupling from GaN to the TiO_2 microstructures.[17] Here we show that TiO_2 nanostructures can also be used to enhance the extraction of the light by reducing the TIR. An enhanced scattering mechanism is proposed, which is newly considered and might be a supplement to the existing microscale and nanoscale processes for light extraction enhancement. We show that although the dielectric nanoparticles have poor light extraction properties, mainly assignable to their small Rayleigh scattering cross-sections, a thick stacking of dense nanoparticles with a nanoscale porosity can greatly enhance the light extraction ability from the substrate they covered, and can be used to enhance the light output of LED significantly. We fabricated TiO_2 nanoparticle films by depositing gas-phase synthesized nanoparticles at room temperature in a vacuum so that degradation of the electrical properties of the p-electrodes can be avoided. It provides an important new approach with potentials for various optoelectronics applications.

Experimental

The oblique deposition technique has been widely used in physical vapor deposition to fabricate porous thin films by controlling the incident trajectory of atoms generated by vacuum evaporation or sputtering. Here we extend the oblique deposition arrangement to the cluster beam deposition process to generate hierarchical nanostructures. A scheme of the oblique angle cluster beam deposition process is shown in Fig. 1. In the oblique angle cluster beam deposition process, a nanoparticle randomly distributed on the substrate produces a shadow region that the incident cluster flux cannot reach, and a non-shadow region where the incident cluster flux deposits preferentially, as shown in Fig. 1(b). As a result, the nanoparticles pile up and form a nanoparticle-based film with orientated nanoscale porosity. In our fabrication, the TiO_2 nanoparticle films were grown by depositing titanium nanoparticles in a high vacuum and then treated with post-oxidation.

Ti nanoparticles were generated in a magnetron plasma gas aggregation cluster source,[18–22] as shown in Fig. 1(a). The magnetron discharge was operated in an argon stream at a pressure of about 100 Pa in a liquid nitrogen cooled aggregation tube. Ti atoms were sputtered from the target and Ti clusters were formed through the aggregation process in the argon gas. The Ti clusters were swept by the gas stream out of the aggregation tube into vacuum through a diaphragm, where the cluster growth was effectively stopped. The clusters continued to pass through a skimmer (the second diaphragm) into a high vacuum chamber and a collimated beam of clusters was formed. In the high vacuum chamber, the Ti clusters were deposited on the substrates that were tilted at a large angle with respect to the cluster beam direction. Post-oxidation of titanium nanoparticles was carried out by exposing the as-deposited film to O_2 at room temperature. Due to the high reactivity of the Ti nanoparticles with O_2, TiO_2 nanoparticles were formed, which was verified with X-ray photoelectron spectroscopy (XPS, ESCALABMK-II). With a number of circular deposition/oxidation steps, a TiO_2 nanoparticle film of the preliminary thickness was prepared. The microstructures of the TiO_2 nanoparticles were characterized using a transmission electron microscope (TEM, FEI TECNAI F20s TWIN) and a Raman spectrometer (NT-MDT NTEGRA spectra), and the morphology of the TiO_2

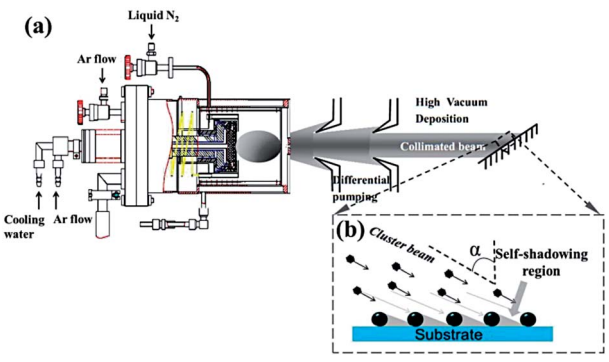

Fig. 1 (a) Schematic diagram of a magnetron plasma gas aggregation cluster source and the gas-phase cluster beam deposition process. (b) Sketch illustrating the oblique angle cluster beam deposition process, where α is the cluster beam incident angle measured from the substrate normal.

nanoparticle films was characterized with scanning electron microscopy (SEM, Hitachi S4500).

To investigate the light extraction property of the porous nanoparticle films, TiO_2 nanoparticles were deposited on the surface of the hemispherical glass prisms at different incident angles. The experimental setup for TIR light extraction analysis is shown in Fig. 2. The bottom of the hemispherical glass prism covered with TiO_2 nanoparticles on its surface was illuminated from its inner side with a beam of collimated white-light passing through the prism. Far-field transmission spectra were collected from the bottom surface of the prism. An integrating sphere was used to collect the light from the prism surface. The light was sent to the spectrometer (Zolix Omni-λ 300) *via* an optical fibre. Both the prism and the integrating sphere were installed on a home-made scanning stage so that the incident angles of the illumination can be varied to generate a TIR geometry.

The porous TiO_2 nanoparticle films were applied for light extraction enhancement of GaN-based LEDs. We measured the light output of GaN LEDs both with photoluminescence (PL) and electroluminescence (EL). The GaN-based LED chips were grown on sapphire substrates with *c*-face orientation (0001) by metal organic chemical vapor deposition (MOCVD). The LED structure consists of a 2 μm thick unintentionally doped GaN layer, a 2 μm thick n-type GaN layer, active layers consisted of eight-period InGaN/GaN multiple quantum wells (MQWs) each with a 3 nm thick InGaN well layer and a 10 nm thick GaN barrier layer, and a 0.3 μm thick p-type GaN layer. PL measurements were carried out by exciting the LED sample from the bottom side of the sapphire substrate with a 405 nm laser diode and collecting PL signals from the obverse side which has the TiO_2 nanoparticle layers. The TiO_2 nanoparticles were directly deposited on top of the p-GaN layer without an ITO electrical contact layer. For EL measurement, the LED sample also consists of a 300 nm thick ITO layer evaporated onto the surface to serve as the upper electrical contact. The TiO_2 nanoparticle coating was deposited on top of the ITO electrical contact layer.

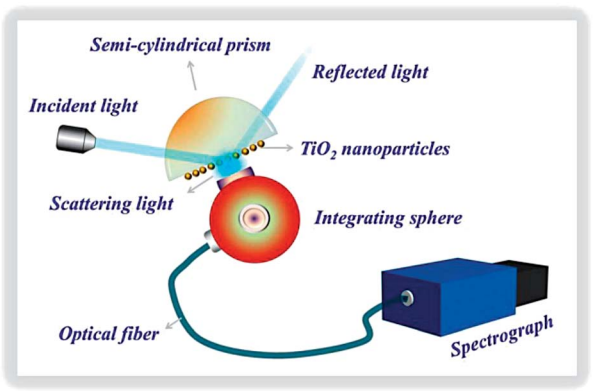

Fig. 2 Experimental setup for the analysis of the extraction of light beyond the critical angle of total internal reflection with TiO_2 nanoparticle films.

Results and discussion

Characterization of the TiO_2 nanoparticle film

The TEM microimage of the TiO_2 nanoparticles is shown in Fig. 3(a). The average diameter of the nanoparticles is measured to be ~8.5 nm. The nanoparticles are randomly distributed on the substrate with a uniform size and little aggregation. XPS spectra of the TiO_2 nanoparticle films shown in Fig. 3(b) indicate that stoichiometric TiO_2 nanoparticles are formed following circularly deposition/oxidation steps. As shown, the binding energies of Ti $2p_{3/2}$ and $2p_{1/2}$ core levels for the sample are 458.3 eV and 576.5 eV respectively, which agree well with the corresponding literature value[23] for TiO_2. The crystalline phase of the TiO_2 nanoparticles was characterized by Raman spectroscopy, and the results are shown in Fig. 3(d). Four Raman-active modes of E_g (142 cm^{-1}), B_{1g} (397 cm^{-1}), A_{1g} (515 cm^{-1}) and E_g (637 cm^{-1}) are observed in the as-deposited TiO_2 nanoparticle film, indicating that the samples consisted of anatase TiO_2 nanocrystals.[24]

Fig. 4 shows the top-view SEMs of the TiO_2 nanoparticle films obliquely deposited on the silica glass surface with various incident angles. The thicknesses of the films were controlled to be 300 nm. It is obvious that the porosity of the nanoparticle films increases with the incident angle of the cluster beam, due to the increase in the area of the shadow region where the incident cluster beam cannot reach.[25–28]

In the oblique cluster beam deposition, the subsequent incident cluster beam would deposit preferentially in the region already covered by nanoparticles. The shadowing effect dominates the film growth process, resulting in extremely porous

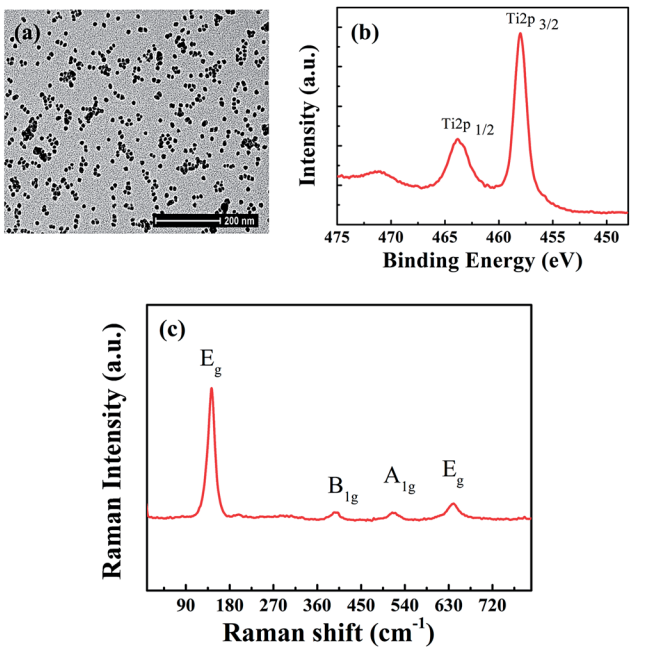

Fig. 3 (a) TEM image of TiO_2 nanoparticles generated from the cluster source. (b) XPS spectra of TiO_2 nanoparticle films. The spectra are referenced to the C1s peak at 285.0 eV. (c) Raman spectra of the as-deposited TiO_2 nanoparticles.

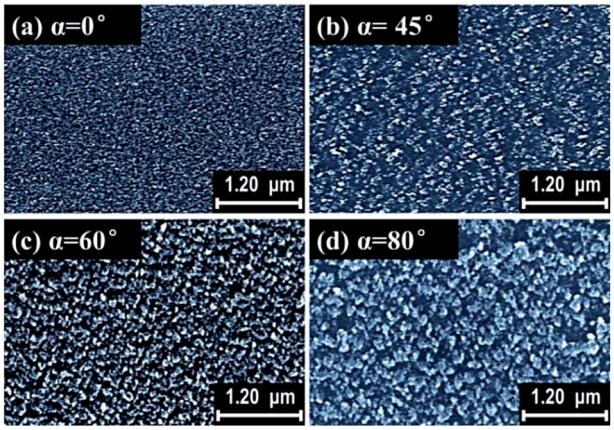

Fig. 4 Top-view SEM images of TiO_2 nanoparticle films deposited on silica substrates by using oblique cluster beam deposition with incident angles of (a) 0°, (b) 45°, (c) 60°, and (d) 80°.

and columnar nanoparticle piling.[29–33] However, in any case, the sizes of the pores distributed in the nanoparticle films are below 50 nm, which are much smaller than the wavelength of the visible light.

The refractive indices of the TiO_2 nanoparticle films obtained by performing ellipsometry measurements and Cauchy model[34] fitting are shown in Fig. 5(a). The Cauchy model expresses the refractive index of a film as:

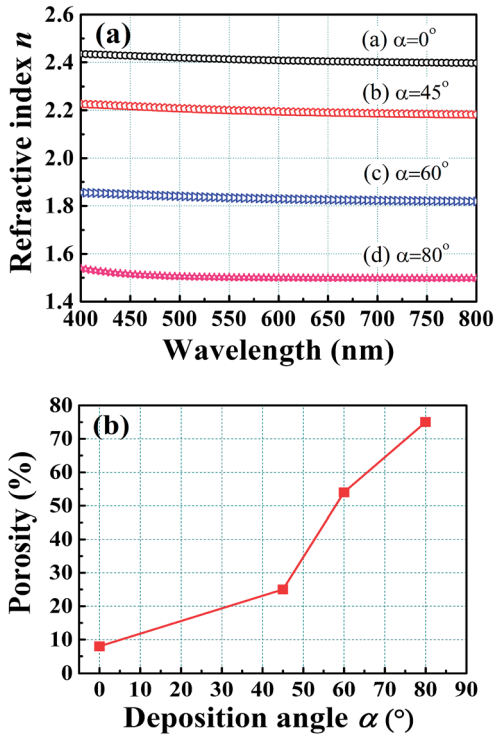

Fig. 5 (a) Measured refractive index of TiO_2 nanoparticle films obliquely deposited on silicon substrates with incident angles (a) 0°, (b) 45°, (c) 60°, and (d) 80°. The calculated porosities of each films are plotted in (b).

$$n_{\text{film}}(\lambda) = A_n + \frac{B_n}{\lambda^2} + \frac{C_n}{\lambda^4} \quad (1)$$

where A_n, B_n and C_n are constants. The refractive index decreases with the increase of the deposition angle α, owing to the increased porosity (a fraction of the volume of the voids over the total volume) of the nanoparticle films. Quantitatively, the refractive index of a porous TiO_2 nanoparticle film is determined by the porosity of the film and the refractive index of bulk TiO_2. The Bruggemann effective medium approximation gives the effective refractive index of a porous TiO_2 film consisting of two components, air and dense TiO_2, with volume fractions V_{air} and V_{TiO_2}, where $V_{\text{air}} + V_{\text{TiO}_2} = 1$. From the measured refractive index, the porosity of the nanoparticle films can be calculated using the following equation:[35]

$$\text{Porosity}(\%) = \left(1 - \frac{{n_{\text{film}}}^2 - 1}{{n_{\text{TiO}_2}}^2 - 1}\right) \times 100 \quad (2)$$

where $n_{\text{TiO}_2}(\approx 2.52)$ is the refractive index of pore-free anatase TiO_2,[36] and n_{film} is the refractive index of the porous nanoparticle films. The calculated porosities corresponding to each incident angles are also indicated in Fig. 5(b). As expected, the porosity of the TiO_2 nanoparticle films decreases as the incident angle increases.

Analysis of the extraction of the light trapped due to total internal reflection

To measure the extraction efficiency of light trapped beyond the TIR critical angle, the TiO_2 nanoparticle films were deposited on prisms made of silica glass. The transmission spectra of light extracted from the hemispherical glass prism with the porous TiO_2 nanoparticle films were characterized by collecting the light emitted to air from the bottom surface of the prism illuminated with collimated white-light propagating in the prism at an incident angle greater than the critical angle of total internal reflection. No light transmission was observable under the same conditions from the bare bottom surface of the hemispherical glass prism. When the surface was covered with TiO_2 nanoparticle films, a significant amount of light otherwise trapped due to TIR could be extracted, which was visible even with naked eye.

The results presented in Fig. 6(a) show the transmittance of light measured beyond the critical angle (45°). It clearly demonstrates that the presence of the TiO_2 nanoparticle films indeed enables the extraction of light otherwise trapped in the prism medium. The transmittance of the light is found to sensitively depend on the wavelength as well as the porosity of the nanoparticle film. Significant light extraction appears at a short wavelength. Below 500 nm, the transmittance of the TIR light increases rapidly with the decrease of the wavelength. On the other hand, the transmittance is more than doubled by increasing the porosity from 25% to 75%. With a 300 nm thick TiO_2 nanoparticle film of 75% porosity (corresponding to a cluster beam incident angle $\alpha = 80°$), more than 4% trapped light can be extracted out at a 455 nm wavelength

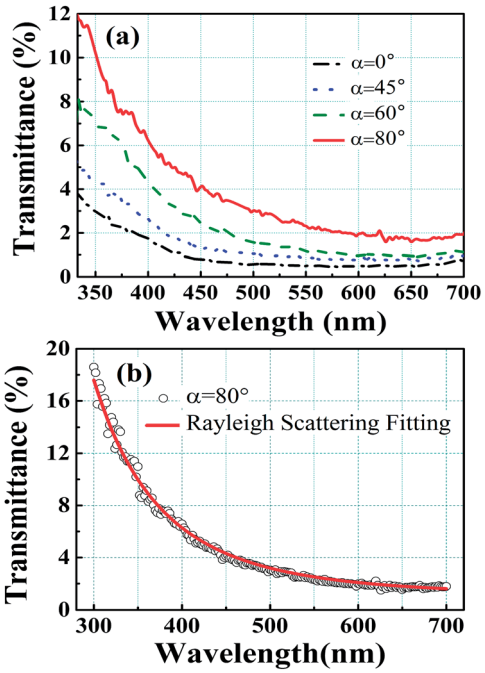

Fig. 6 (a) Spectral transmittance of light extracted from the hemispherical glass prisms for a 50° angle of light incidence. The surfaces of the prisms are covered with TiO_2 nanoparticle films deposited at different oblique incident angles. (b) Rayleigh scattering fitting of the measured transmittance.

(corresponding to the typical emission wavelength of a GaN-based LED).

There are a number of approaches aimed to extract the light trapped inside the medium due to total internal reflection. Random surface texturing or roughening at microscale or submicroscale has been proven to be an effective way[37] to reduce internal light reflection and the effect can be modelled with ray tracing.[38] In the present study, the size of the nanoparticles and the gaps between the nanoparticle columns are much smaller than the wavelength of visible light, which implies that the nanoparticle layer can be treated as a single homogeneous film with a uniform refractive index and the light extraction is not dominated by the effect of the texturing of the surface. To interpret the light extraction enhancement observed in the present experiment, we propose a scattering mechanism of the porous nanoparticle layers. Since the refractive index of the TiO_2 nanoparticle is much larger than that of air, and even larger than that of silica, the substrate modes are largely interrupted, those light rays which are otherwise totally reflected can escape from the silica substrate and enter the TiO_2 nanoparticle coating. In the random distribution of nanoparticles and nano-sized pores, light scattering will occur due to refractive index fluctuations throughout the nanoparticle layer. Detailed analysis has shown that scattering structures will be most effective in extracting light when located at the medium–air interface.[11]

It was found that the measured transmittance could be well fitted with a function proportional to $1/\lambda^4$, as shown in Fig. 6(b), which suggests that the mechanism for light extraction is based on Rayleigh scattering. According to Rayleigh,[39] the cross-section of elastic scattering of light by particles much smaller than the wavelength of the light is given by:

$$\sigma_{sca} = \frac{2\pi^5}{3}\frac{d^6}{\lambda^4}\left(\frac{n^2-1}{n^2+1}\right)^2 \quad (3)$$

where d is the diameter of the particle and n is the refractive index of the particle. For the aggregated nanoparticles with columnar structures, the Rayleigh scattering cross-section becomes:[40]

$$\sigma_{sca} = \frac{8\pi^3}{3}\frac{V^2}{\lambda^4}(n^2 - n_{air}{}^2)^2 \quad (4)$$

where V is the mean volume of the columnar aggregation of nanoparticles and n_{air} is the refractive index of air, $n_{air} = 1$. Eqn (4) indicates that the volume of columnar aggregation and the refractive index of the nanoparticles determined the Rayleigh scattering cross-section. For the porous TiO_2 nanoparticle film with columnar particle aggregations fabricated by glancing-angle deposition, a larger incident deposition angle leads to larger nanoparticle agglomerate columns and higher porosity of the films. Therefore the Rayleigh scattering cross-sections increase with the deposition angle. The tendency of columnar aggregation of nanoparticles in the porous layer results in excess optical scattering, *i.e.*, the scattering power will be larger than the sum of the Rayleigh scattering cross-section of the individual nanoparticles due to the coherent scattering from the particles that are very closely piled with each other. The strong contrast in the refractive index between pores and nanoparticles further results in very strong scattering. The scattering efficiency is maximized when the refractive index contrast between the scattering elements and air is large so that high refractive index materials such as TiO_2 are preferred.

Light output enhancement of LEDs

We investigated the enhancement of the light output of the GaN LED with porous TiO_2 nanoparticle coatings both with PL and EL measurements. TiO_2 nanoparticle films were fabricated on top of the GaN-LED wafer by oblique cluster beam deposition with an incident angle $\alpha = 80°$. The thickness of the TiO_2 nanoparticle films was about 300 nm. Fig. 7(b) compares the PL emission spectra of the GaN wafers with and without a TiO_2

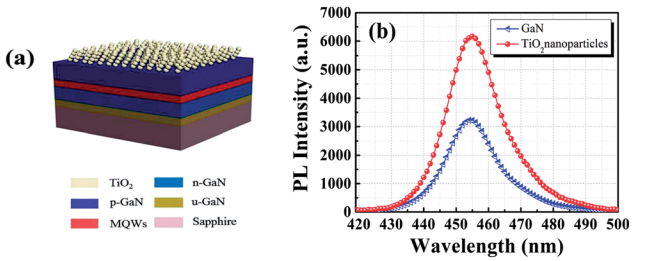

Fig. 7 (a) Schematic device structure of a GaN wafer coated with TiO_2 nanoparticle layers used for PL measurement. (b) A comparison of the room temperature PL intensity between bare GaN LEDs and GaN LEDs covered with TiO_2 nanoparticle layers.

nanoparticle layer. The PL spectrum of the GaN wafer constructed with a TiO_2 nanoparticle layer is not distorted but the PL intensity is much increased, up to 92% stronger than that of the bare GaN wafer, which is basically consistent with that estimated based on the results of the prism experiment. For a planar LED, the light extraction efficiency η_e can be estimated to be $1/4n^2$.[41] The refractive index of GaN is $n = 2.5$, so that only about 4% emission light can be extracted out in a GaN-LED. For LED light output enhancement, although only several percent (4% at 450 nm wavelength in the case of the TiO_2 nanoparticle film deposited with an incident angle $\alpha = 80°$) of trapped light due to TIR can be extracted, the increase of the light output is significant.

It was reported that the multi-layer graded-refractive index anti-reflection coating fabricated by oblique-angle deposition can achieve a significant light-extraction efficiency enhancement due to a strongly reduced Fresnel reflection at the semiconductor–air interface.[13] In such a coating, each layer has a refractive index that is individually tuned to form a stack with the refractive index graded from its dense materials value down to the value close to that of air for an optimum anti-reflection performance. For the TiO_2 nanoparticle layer we fabricated, the effective refractive index is well above the refractive index of air so that optimum anti-reflection is not achieved. The enhancement of the light-extraction efficiency is not dominated by the reduction of Fresnel reflection. Instead, scattering induced by refractive index fluctuations among the TiO_2 nanoparticle layer is responsible for the light output enhancement mechanism, as confirmed by the prism experiments.

Fig. 8(b) shows the EL spectra measured at an injection current of 20 mA. Fig. 8(c) shows the EL intensity *versus* current characteristics of a GaN LED with the TiO_2 nanoparticle coating, with a comparison to that of a conventional GaN-LED. Similar to the PL emission, a little distortion on the spectrum of the EL emission can be observed after coating the TiO_2 nanoparticle layer, however, there are obvious enhancements of the EL intensities at all the injection currents. The light output of the LED with the TiO_2 nanoparticle coating is about 30% higher than that of the conventional LED at an injection current of 20 mA. However, comparing with the PL measurement, the enhancement of EL spectra of the GaN LED is largely reduced. Considering the fact that a lower refractive index ITO layer which may contain some surface roughness is introduced between GaN and TiO_2 in the EL measurement, such a reduction in the light output enhancement is reasonable. Due to the insertion of the ITO layer, TIR at the GaN–ITO interface induces a large fraction of light being trapped in the GaN layer. Only the light that escapes from the GaN to the ITO layer can be affected by the enhanced extraction of the TiO_2 nanoparticle coating.

The current–voltage (*I–V*) characteristics of GaN LEDs with and without TiO_2 nanoparticle coatings are plotted in Fig. 8(d). As shown, the forward voltage of LEDs is 3.42 V at a driving current of 20 mA, which is not altered after TiO_2 coating. It implies that the TiO_2 nanoparticle deposition does not deteriorate the electrical properties of the LED chips. In contrast, surface texturing fabricated with lithography and etching usually generates degradations on the electrical properties of

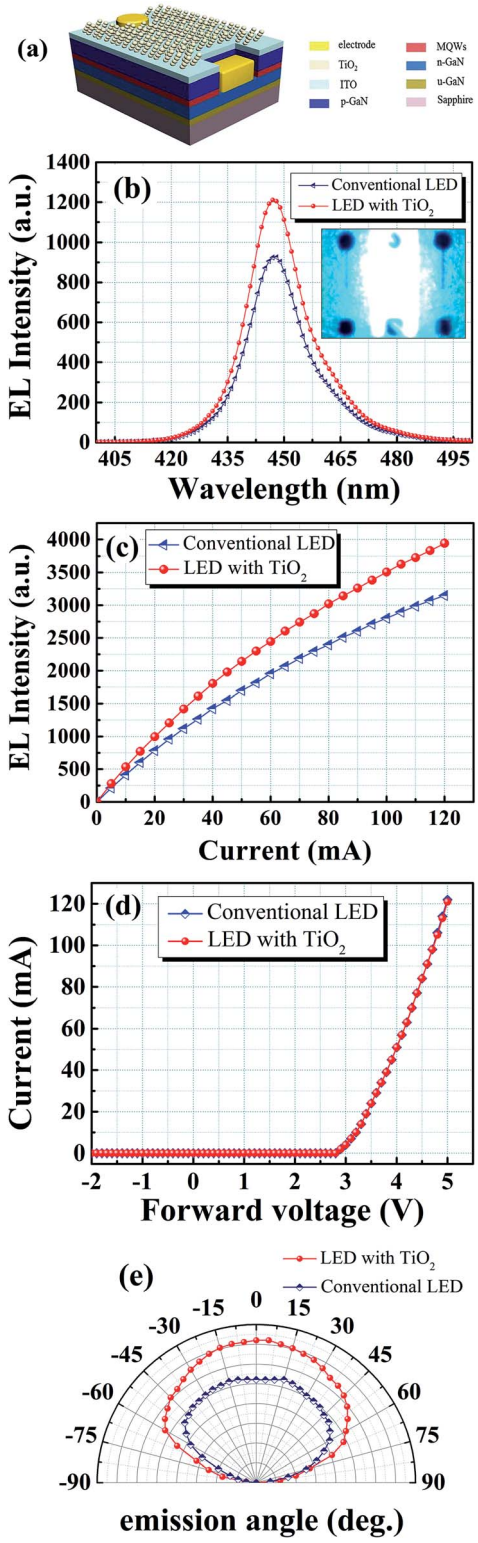

Fig. 8 (a) Schematic device structure of a GaN-LED chip coated with TiO_2 nanoparticle layers used for EL measurement. (b) EL spectra measured at 20 mA injection current. The inset shows a photograph of the devices under operation. (c) EL intensity *versus* current characteristics of GaN LEDs with and without TiO_2 nanoparticle coatings. (d) A comparison of the current–voltage characteristics of GaN LEDs with and without TiO_2 nanoparticle layers. The two curves are completely overlapped. (e) The radiation profile of the two kinds of LEDs under a 20 mA injection current.

the LED. Fig. 8(e) shows the radiation profiles of the conventional LEDs and LEDs with TiO_2 nanoparticles. The measurement was performed in the plane that contains the tilted axis of the incident nanoparticle beam. The direction perpendicular to the surface of the LED is defined as zero degree. The light output intensity distribution of the LED with TiO_2 nanoparticle layers measured in the angular range of -70° to 70° is clearly enhanced compared to the conventional LED. The light intensity enhancement at the whole angular range is relatively homogeneous. But a little directed enhancement can be observed toward the vertical direction. Clearly the light extraction enhancement has no significant correspondence with the oblique angle of nanoparticle columns in the porous TiO_2 nanoparticle film. This indicates that the waveguiding effect observed for nanorod arrays[15,18] plays a small role in the light extraction enhancement of the present TiO_2 nanoparticle film, due to the inhomogeneous granular nature of the TiO_2 nanoparticle columns. Instead, the nearly omnidirectional enhancement of the light output can be explained with the scattering effect of the TiO_2 nanoparticle porous layer. We also note here that the enhanced light extraction with the TiO_2 nanoparticle porous layers can function with the microscale surface texturing in parallel to generate an additional enhancement. We have observed a significantly enhanced extraction of light from the substrate surface that had microscale texturing by obliquely depositing TiO_2 nanoparticle layers. Therefore, the purpose of using the nanoparticle based light extraction layers is to provide a supplement to the microscale texturing structures, rather than to replace them.

Conclusions

In summary, porous TiO_2 nanoparticle layers were fabricated with gas phase cluster beam deposition at glancing incidence. The fabricated nanoparticle based films are composed of columnar TiO_2 nanoparticle piles separated with nanoscale pores. The porosity as well as the refractive index of the nanoparticle layers can be precisely tuned by the incident angle of deposition. The TiO_2 nanoparticle layers were deposited on the bottom surface of the hemispherical glass prism to investigate the light extraction under total internal reflection. Effective extraction of the light trapped in the substrate due to TIR with the TiO_2 nanoparticle layers was demonstrated. The transmittance of the light under the TIR conditions was found to increase rapidly with the porosity, which can be raised by adopting a larger incident angle of cluster deposition. The transmission spectrum was found to vary inversely with the fourth power of the wavelength, indicating that the mechanism for light extraction is based on Rayleigh scattering. The columnar aggregation of the nanoparticles as well as the strong contrast in the refractive index between pores and TiO_2 nanoparticles in the nanoporous structures results in very strong light scattering. At 450 nm wavelength, 4% light which is otherwise trapped by TIR could be extracted from the silica glass substrate by using a TiO_2 nanoparticle layer with 75% porosity. The porous TiO_2 nanoparticle coatings were fabricated on the surface of GaN LEDs to enhance their light output. A nearly 92% enhancement of the PL intensity as well as a 30% enhancement of the EL intensity was observed. The strategy of our current enhanced light extraction demonstrates an alternative mechanism for LED light output enhancement, which has the advantage that it induces no alterations in the electrical properties of the LEDs and can function with the microscale surface texturing in parallel to generate an additional enhancement.

Acknowledgements

The authors thank the National Natural Science Foundation of China (Grant no. 51171077, 11304159), the National Basic Research Program of China (973 Program, Grant no. 2014CB932302, 2009CB930501) and the Scientific Research Foundation of Graduate School of Nanjing University (Grant no. 2013CL10). This research was also supported by a project funded by the Priority Academic Program Development of Jiangsu Higher Education Institutions.

Notes and references

1 D.-S. Tsai, C.-A. Lin, W.-C. Lien, H.-C. Chang, Y.-L. Wang and J.-H. He, *ACS Nano*, 2011, **5**, 7748–7753.
2 H.-P. Wang, T.-Y. Lin, C.-W. Hsu, M.-L. Tsai, C.-H. Huang, W.-R. Wei, M.-Y. Huang, Y.-J. Chien, P.-C. Yang and C.-W. Liu, *ACS Nano*, 2013, **7**, 9325–9335.
3 R. Horng, C. Yang, J. Wu, S. Huang, C. Lee and D. Wuu, *Appl. Phys. Lett.*, 2005, **86**, 221101–221103.
4 J.-K. Sheu, Y. Lu, M.-L. Lee, W.-C. Lai, C. Kuo and C.-J. Tun, *Appl. Phys. Lett.*, 2007, **90**, 263511–263513.
5 S. Zhu, A. Yu, D. Hawley and R. Roy, *Am. J. Phys.*, 1986, **54**, 601.
6 A. Chutinan, K. Ishihara, T. Asano, M. Fujita and S. Noda, *Org. Electron.*, 2005, **6**, 3–9.
7 G. Gu, D. Garbuzov, P. Burrows, S. Venkatesh, S. Forrest and M. Thompson, *Opt. Lett.*, 1997, **22**, 396–398.
8 X. Liu, W. Zhou, Z. Yin, X. Hao, Y. Wu and X. Xu, *J. Mater. Chem.*, 2012, **22**, 3916–3921.
9 J. K. Sheu, I. Hung, W. C. Lai, S. C. Shei and M. Lee, *Appl. Phys. Lett.*, 2008, **93**, 103503–103507.
10 Y. Gao, T. Fujii, R. Sharma, K. Fujito, S. P. Denbaars, S. Nakamura and E. L. Hu, *Jpn. J. Appl. Phys.*, 2004, **43**, L637–L639.
11 J. K. Kim, S. Chhajed, M. F. Schubert, E. F. Schubert, A. J. Fischer, M. H. Crawford, J. Cho, H. Kim and C. Sone, *Adv. Mater.*, 2008, **20**, 801–804.
12 S. J. An, J. H. Chae, G.-C. Yi and G. H. Park, *Appl. Phys. Lett.*, 2008, **92**, 121103–121108.
13 Y.-H. Hsiao, C.-Y. Chen, L.-C. Huang, G.-J. Lin, D.-H. Lien, J.-J. Huang and J.-H. He, *Nanoscale*, 2014, **6**, 2624–2628.
14 H. Gao, F. Yan, Y. Zhang, J. Li, Y. Zeng and G. Wang, *J. Appl. Phys.*, 2008, **103**, 014314–014315.
15 J. Zhong, H. Chen, G. Saraf, Y. Lu, C. Choi, J. Song, D. Mackie and H. Shen, *Appl. Phys. Lett.*, 2007, **90**, 203513–203515.

16 C.-H. Ho, Y.-H. Hsiao, D.-H. Lien, M. Tsai, D. Chang, K.-Y. Lai, C.-C. Sun and J.-H. He, *Appl. Phys. Lett.*, 2013, **103**, 161104.
17 X.-H. Li, P. Zhu, G. Liu, J. Zhang, R. Song, Y.-K. Ee, P. Kumnorkaew, J. F. Gilchrist and N. Tansu, *J. Disp. Technol.*, 2013, **9**, 324–332.
18 H. Haberland, M. Mall, M. Moseler, Y. Qiang, T. Reiners and Y. Thurner, *J. Vac. Sci. Technol., A*, 1994, **12**, 2925–2930.
19 M. Han, C. Xu, D. Zhu, L. Yang, J. Zhang, Y. Chen, K. Ding, F. Song and G. Wang, *Adv. Mater.*, 2007, **19**, 2979–2983.
20 M. Y. Zheng, W. Y. Li, M. J. Xu, N. Xu, P. Chen, M. Han and B. Xie, *Nanoscale*, 2014, **6**, 3930–3933.
21 L. B. He, X. Chen, Y. W. Mu, F. Q. Song and M. Han, *Nanotechnology*, 2010, **21**, 495601.
22 K. Wegner, P. Piseri, H. V. Tafreshi and P. Milani, *J. Phys. D: Appl. Phys.*, 2006, **39**, R439.
23 A. S. Zuruzi and N. C. MacDonald, *Adv. Funct. Mater.*, 2005, **15**, 396–402.
24 W. Zhang, Y. He, M. Zhang, Z. Yin and Q. Chen, *J. Phys. D: Appl. Phys.*, 2000, **33**, 912.
25 C. H. Chang, P. Yu and C. S. Yang, *Appl. Phys. Lett.*, 2009, **94**, 051114.
26 S. Wang, G. Xia, H. He, K. Yi, J. Shao and Z. Fan, *J. Alloys Compd*, 2007, **431**, 287–291.
27 J. Q. Xi, J. K. Kim, E. F. Schubert, D. Ye, T. M. Lu, S.-Y. Lin and J. S. Juneja, *Opt. Lett.*, 2006, **31**, 601–603.
28 J. Q. Xi, M. F. Schubert, J. K. Kim, E. F. Schubert, M. Chen, S. Y. Lin, W. Liu and J. A. Smart, *Nat. Photonics*, 2007, **1**, 176–179.
29 M. M. Hawkeye and M. J. Brett, *J. Vac. Sci. Technol., A*, 2007, **25**, 1317–1335.
30 S. R. Kennedy and M. J. Brett, *Appl. Opt.*, 2003, **42**, 4573–4579.
31 P. Mao, J. Chen, Y. Zhou, K. Liao, B. Zhao, J. Han, G. Wang and M. Han, *Phys. Status Solidi C*, 2012, **9**, 2366–2369.
32 D. Vick, L. Friedrich, S. Dew, M. Brett, K. Robbie, M. Seto and T. Smy, *Thin Solid Films*, 1999, **339**, 88–94.
33 C. Zhou and D. Gall, *J. Appl. Phys.*, 2008, **103**, 014306–014307.
34 Y. Liu, J. Hsieh and S. Tung, *Thin Solid Films*, 2006, **510**, 32–38.
35 B. E. Yoldas and D. P. Partlow, *Thin Solid Films*, 1985, **129**, 1–14.
36 W. D. Kingery, H. K. Bowen, D. R. Uhlmann, *Introduction to Ceramics*, Wiley, New York, 1976, pp. 650–651.
37 A. I. Zhmakin, *Phys. Rep.*, 2011, **498**, 189–241.
38 S. J. Lee, *Appl. Opt.*, 2001, **40**, 1427–1437.
39 J. W. Strutt, *London, Edinburgh Dublin Philos. Mag. J. Sci.*, 1871, **41**, 447–454.
40 S. Kassam, I. J. Hodgkinson and S. C. Cloughley, *J. Opt. Soc. Am. A*, 1995, **12**, 2009–2021.
41 X. Sheng, L. Z. Broderick, J. Hu, L. Yang, A. Eshed, E. A. Fitzgerald, J. Michel and L. C. Kimerling, *Opt. Express*, 2011, **19**, A701–A709.